STRATEGIC ASTROPHYSICS TECHNOLOGY

Technology Milestone White Paper

*Laboratory Demonstrations of High Contrast
with Black Silicon Coronagraph Masks*

A J Eldorado Riggs[1]
Garreth J. Ruane[1]
Gregory W. Allan[1]
Kunjithapatham Balasubramanian[1]
Karl Y. Yee
Victor E. White
Ewan S. Douglas[2]
Ramya M. Anche[2]
Emory L. Jenkins[2]

[1]Jet Propulsion Laboratory, California Institute of Technology
[2]University of Arizona

24 June 2024

Approvals:

Released by

_____   _____
A J Eldorado Riggs   **Date**
Principal Investigator

Approved by

_____   _____
Brendan Crill   **Date**
ExEP Deputy Chief Technologist, JPL

_____   _____
Nick Siegler   **Date**
ExEP Chief Technologist, JPL

_____   _____
Lucas Paganini   **Date**
ExEP Executive, NASA HQ

Table of Contents

1   Introduction

The Decadal Survey on Astronomy and Astrophysics 2020 (Astro2020) recommends that NASA's next large flagship mission be designed to spectrally characterize at least 25 potentially habitable exoplanets. This 6-meter, space-based, infrared/optical/ultraviolet observatory will likely have a segmented aperture. The typical approach for reaching high contrast on segmented apertures is pupil apodization. But to date, the best broadband contrast that reflective apodizer masks have achieved is 4×10^{-9}. Those black silicon apodizers were designed for the Roman Space Telescope Coronagraph Instrument and were inherently limited by large telescope pupil obscurations. With new designs for a friendlier, off-axis telescope pupil, black silicon apodizers should be able to provide the 10^{-10} contrast needed to image and characterize Earth-like exoplanets. This project will perform testbed demonstrations and model validation to prove this capability.

1.1   Background

In order to spectrally characterize at least 25 potentially habitable exoplanets and advance general astrophysics, the Astro2020 recommended that NASA's next major flagship mission be a 6-meter, off-axis, infrared/optical/ultraviolet (IROUV) telescope, currently referred to as the Habitable Worlds Observatory (HWO). Two flagship mission concept studies focusing on Earth-like exoplanet characterization informed Astro2020—the Habitable Exoplanet Observatory (HabEx) and the Large Ultraviolet Optical Infrared Surveyor (LUVOIR).

The main challenge of directly imaging habitable exoplanets is overcoming diffraction. The planet-to-star flux ratio is approximately 10^{-10} in reflected visible light for an Earth-like planet around a sun-like star. Even for the closest stellar systems, the on-sky separation is just a fraction of an arcsecond. The tails of the stellar point spread function (PSF) completely overwhelm the exoplanet signal in a regular, unmasked image.

A stellar coronagraph is a set of specialized masks and mirrors downstream of a telescope that suppresses starlight while still passing off-axis light from scientific targets such as exoplanets. There are many proposed coronagraphic architectures, and they vary based on how they manipulate the phase and/or amplitude of light in one or more optical planes.

Segment gaps and obscurations in a telescope pupil generate more diffraction in the focal plane that coronagraphs must reject, and the proposed 6-meter HWO flagship is likely to have a segmented aperture to reduce mass and cost. A powerful design tool for mitigating this extra diffraction is pupil apodization. In fact, both the on-axis LUVOIR-A and off-axis LUVOIR-B concepts utilize pupil apodization in their coronagraph designs as illustrated in Figure 1-1, so it is reasonable to assume that pupil apodization would be strongly considered as part of the HWO coronagraph design. It is also worth noting that pupil apodization is versatile and can be paired with any type of focal plane mask (FPM)—LUVOIR-A uses an apodized pupil Lyot coronagraph (APLC) and LUVOIR-B uses an apodized vortex coronagraph (AVC).
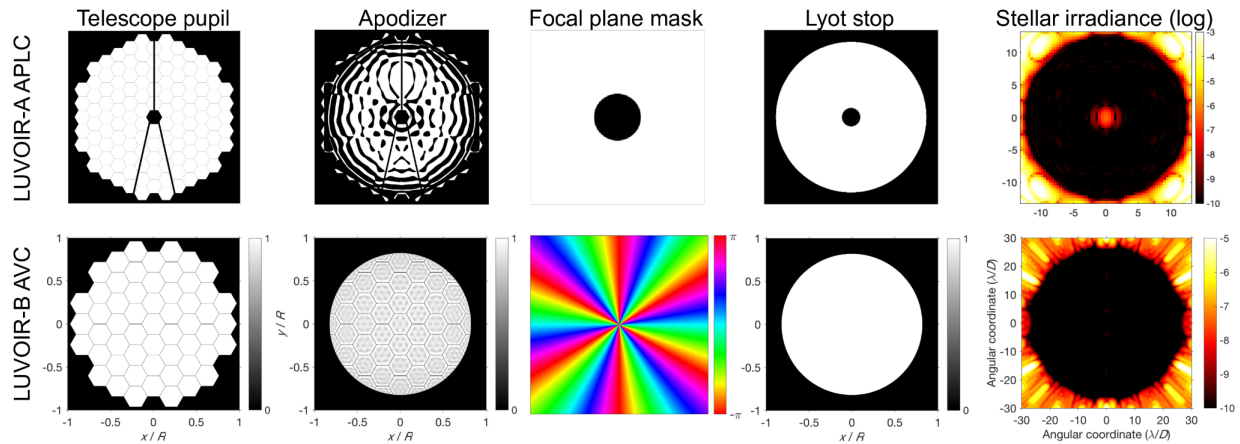
Figure 1-1. Apodization is used to suppress segment gap diffraction in both proposed LUVOIR architectures. Top row: One of the baselined APLC designs for LUVOIR-A (Juanola-Parramon et al. 2019). Bottom Row: An AVC design for LUVOIR-B (Ruane et al. 2018).

The best path forward for amplitude apodizers is with reflective masks due to their achromaticity. To date, the best lab performance for a reflective apodizer was demonstrated by the Roman Space Telescope (Roman) Coronagraph Instrument (CGI). Cady et al. (2017) and Marx et al. (2018) separately demonstrated 4×10^{-9} contrast in >=10% spectral bandwidths with these black silicon apodizers. Because of the large obscurations of the Roman pupil, those coronagraph designs were inherently limited to >10^{-9} contrast and low throughput as found in extensive mask design surveys (Riggs et al. 2017, Gersh-Range et al. 2022). With an off-axis aperture, an apodizer design could provide both higher contrast and higher throughput.

1.2   Objectives and Expected Significance

1.2.1 Objectives

We have three major technical objectives in this project.

- **Objective 1**: <u>Demonstrate that black silicon apodizers can achieve the broadband contrast levels needed for imaging and characterizing habitable exoplanets.</u> Our goal is <5×10^{-10} contrast in 10% bandwidth light to match the best ever achieved in the same facility. Apodizer designs will be tested for an unobscured aperture in years 1 and 2 and for a segmented aperture in year 3.
- **Objective 2**: <u>Develop and empirically validate a diffraction model for specular reflection off black silicon.</u> This is needed to predict its contribution to the contrast error budget in the coronagraphic dark zone. This will be performed in the first half of year 1.
- **Objective 3**: <u>Develop and empirically validate a vector diffraction model of small features and edges in black silicon apodizers.</u> This is to quantify the contribution to the

contrast error budget of polarization aberrations induced by small mask features. The first vector diffraction modeling and testbed experiments in years 1 and 2 will use only circularly symmetric, 1-D optimized radial mask designs in order to reduce the complexity of the calculations. In year 3, the vector diffraction modeling and lab experiments will switch to 2-D optimized apodizers for a segmented aperture.

1.2.2 Expected Significance

Are we alone? Is the Earth unique? Could other worlds harbor the conditions for life or even life itself? These are some of the driving questions for NASA, and we are at the technological brink of being able to answer them with direct observations of nearby exoplanets. Astro2020 recommends that the next NASA flagship be capable of imaging and spectrally characterizing about 25 potentially habitable exoplanets. This is a challenging task, and Astro2020 determined that a 6-meter diameter, IROUV telescope equipped with a coronagraph instrument is needed. Monolithic primary mirrors are the most suitable for coronagraphs, but the HabEx study found that trying to package and launch a monolith >4 meters in diameter is prohibitively complicated and costly. Therefore, the 6-meter HWO primary mirror will most likely be segmented. Making coronagraphs compatible with segmented apertures could greatly reduce the cost of HWO.

Pupil apodization is a powerful approach for suppressing the diffraction from pupil segmentation gaps. In fact, apodization was baselined in both versions of the segmented-aperture LUVOIR mission concept—in combination with a Lyot coronagraph for LUVOIR-A and with a vortex coronagraph for LUVOIR-B. It is therefore likely that apodization could be in the baseline for the HWO flagship as well. **This proposal aims to demonstrate and characterize apodizer performance near the 10^{-10} contrast level so that apodizers can be a proven, safe technology for characterizing Earth-like exoplanets with the HWO mission concept.**

1.3   Perceived Impact to State of Knowledge

Currently, no single coronagraphic technology is able to provide the 25 spectra of Earth-like exoplanets that Astro2020 wants from HWO. Table 1-1 shows the state-of-the-art performance for three past coronagraphic demonstrations, our proposed demonstrations, and the goals in the Tier 1 gap "Coronagraph Contrast and Efficiency" in the Astrophysics Technology Gap Priority List. To date, the best demonstrated broadband contrast, 4×10^{-10}, was with the classical Lyot coronagraph (CLC) (Seo et al. 2019). Unfortunately, the CLC architecture would give poor system-level performance on HWO. The CLC's strong sensitivity to tip/tilt means that contrast degrades by orders of magnitude when observing partially-resolved stellar disks—essentially all nearby stars for a 6-meter telescope (Pueyo et al. 2019). Other architectures provide the necessary robustness, but their biggest remaining performance gap is contrast. None have demonstrated better than 2×10^{-9} broadband contrast in the lab (Belikov et al. 2007, Trauger et al. 2007, Marx et al. 2018, Ruane et al. 2022).

Table 1-1. State-of-the-art, proposed, and NASA Astrophysics Division (APD) desired performance levels for coronagraphs.

Performance Metric	Past Results			This Project	APD Goals
	CLC (Seo 2018)	Vector Vortex (Ruane 2022)	SPLC for Roman CGI (Marx 2018)	SPLC	Goals from APD Gap List
Contrast	4e-10	1.6e-9	4e-9	< 5e-10	< 1e-10
Core Throughput	12%	24%	5%	>= 10%	>=10%
IWA (λ/D)	3.0	3.0	6.5	<= 4.0	<= 3.0
Spectral Bandwidth	10%	10%	10%	>= 10%	20%
Tip/tilt Robustness	Poor	Good	Good	Good	Good

Ultimately for HWO, a promising path forward to achieve all the Astrophysics Division (APD) performance goals is the development of the AVC since that was the baseline choice for the similar but larger off-axis, segmented pupil of LUVOIR-B. AVC mask development can be cleanly split into two efforts, one for apodizers and one for vector vortex masks. Vector vortex masks are currently funded by an existing Strategic Astrophysics Technology (SAT) award, but reflective apodizers have not previously been funded to reach the contrast needed for HWO. This project fills that gap.

The Roman CGI project invented and matured black silicon apodizers, which have passed all flight qualification testing (i.e., vibration, radiation hardness, and thermal). They reached 4×10^{-9} broadband contrast in tests but then stopped as that was sufficient for that mission. This proposal plans to use that same coronagraph architecture, the shaped pupil Lyot coronagraph (SPLC) (Zimmerman et al. 2016), except with off-axis input pupils to demonstrate better contrast, throughput, and inner working angle (IWA) levels relevant to HWO. These high contrast SPLC results would be groundbreaking because they would be the first demonstration of *any* coronagraph capable of yielding any Earth-like exoplanet spectra if it were placed on a large flagship. In addition, via model validation of apodizers in SPLCs, we would be proving that apodizer performance is predictable in every coronagraph architecture, such as the AVC.

Technology Readiness Level (TRL) is dependent on context. Black silicon apodizers have already been flight qualified, having reached 2×10^{-8} broadband contrast after the Roman CGI thermal vacuum testing in spring 2024. However, these masks are still currently unproven near 10^{-10} contrast and are therefore only at TRL 3 or 4 in the context of HWO. With the proposed laboratory demonstrations and modeling, this project aims to achieve TRL 5 criteria for black silicon apodizers with respect to HWO requirements and environments.

2   Black Silicon Masks

The Jet Propulsion Laboratory's (JPL's) Microdevices Laboratory (MDL) pioneered and matured the combination of lithography and cryogenic black silicon to make flight-qualified apodizers for Roman CGI. This project will use this established fabrication technology to make new apodizers designed with higher performance for potential HWO telescope pupils.

2.1   Apodizers for Coronagraphy

Apodization changes the spatial frequency content of the pupil plane and reshapes the PSF to reduce the relative amount of starlight in some regions. An apodizer can modify the amplitude (Slepian 1965) or phase (Por 2020) of the pupil plane electric field, but this proposal just considers amplitude apodizers because they have much higher technical maturity for high-contrast, space-based applications.

Apodizers as originally considered for astrophysics, such as by Slepian 1965, had smoothly varying amplitude profiles. These partially transmissive designs are infeasible to manufacture directly. Depositing a variable-thickness metal layer on glass is a non-standard fabrication process and results in chromatic amplitude and phase shifts.

A switch to binary-amplitude apodizers was the next improvement toward manufacturable designs. One way of making a design binary in amplitude is the error diffusion method, in which localized regions of a partially transmissive apodizer design are replaced with an equivalent area of binary transmission shapes (Floyd and Steinberg 1976, Dorrer and Zuegel 2007). Another method was to optimize binary apodizations directly, which came to be called shaped pupils (Kasdin 2003). Unfortunately, the highest performance binary amplitude apodizations were not initially considered viable because they contained free-floating obscurations. This meant they could not be made as freestanding, through-hole masks and instead had to be patterned on a substrate. Until 2013, this meant the apodizer had to be a metal-on-glass, transmissive design, which suffers from dispersion and ghosting within the glass substrate.

2.2   Black Silicon

A breakthrough in apodizer fabrication was made by JPL's MDL when they combined different techniques to make binary apodizers for use in reflection (Balasubramanian et al. 2013). Starting with a thick (e.g., 5 mm), highly polished silicon wafer, the regions where starlight is wanted are coated with bare aluminum, and the regions where starlight is to be removed are cryogenically etched downward to form black silicon. Figure 2-1 shows a scanning electron microscope (SEM) image of a small region of a black silicon apodizer mask with square design pixels. The aluminum regions are the flat, rectangular plateaus, and the black silicon looks like a forest of approximately one-micron wide and ten-micron tall needles. The specular reflectance of the black silicon can be so low ($<10^{-7}$) that it is difficult to measure accurately above detector

noise (Balasubramanian et al. 2019). This measurement was made at an 8 degree angle of incidence, which is relevant for testbeds and future instruments because the optics within a coronagraph instrument or testbed generally have <= 10 degree angles of incidence to minimize polarization aberrations. The specular reflectance of black silicon does not dramatically increase until much larger angles of incidence of around 30-40 degrees.
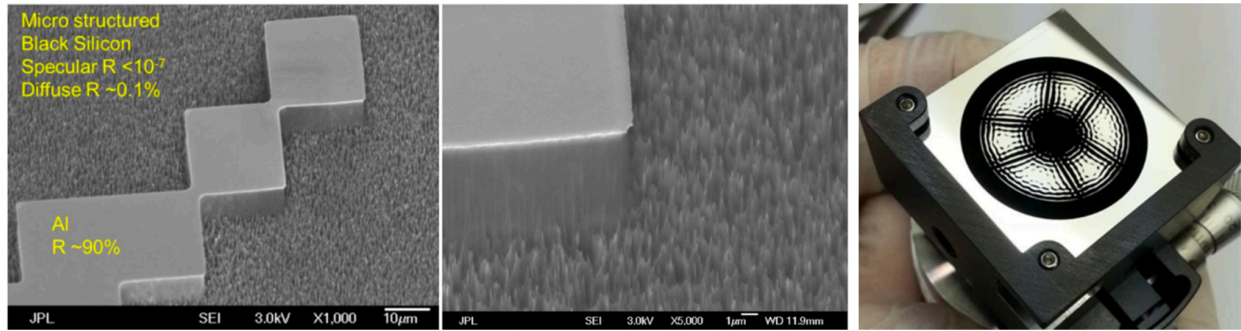
Figure 2-1. (Left and middle) Scanning electron microscope images of a small region of a black silicon apodizer mask. The reflective, aluminum-coated regions appear as plateaus above the forest of absorptive black silicon needles. (Right) Photo of a fabricated black silicon apodizer with a design for Roman CGI (Balasubramanian et al. 2019).

There is good reason to believe that black silicon apodizers will be viable for the full wavelength range desired for HWO, from the near ultraviolet to the near infrared. Bare aluminum is known to have high reflectance over that whole range. Cryogenic black silicon has shown <=0.2% hemispherical reflectance from 0.4-1.0 microns (Balasubramanian et al. 2017), and for a highly doped silicon wafer it can stay black out to 20 microns. The specular reflectance has only been directly measured at 633 nm thus far (Balasubramanian et al. 2017) but is expected to correlate closely with the level of diffuse reflectance. For this project, the apodizers will only be tested in the subset of the visible spectrum that is possible in our existing testbeds.

Compared to the other main reflective apodizer technology, carbon nanotubes (CNTs), black silicon has two main advantages. First, black silicon apodizers were flight qualified (i.e., for radiation hardness and launch vibrations) by the Roman CGI project. Second, black silicon is created with a downward etch in a single piece of silicon. CNTs are grown upward from the mirror surface which results in adhesion problems and an exact height being required to get the correct amount of shadowing for the required non-zero angle of incidence. The best results for CNT apodizers to date are in monochromatic light: 3×10^{-8} contrast in air (Will et al. 2023) and 5×10^{-9} contrast in vacuum (Sirbu et al. 2023).

The Milestone 1 Report for the Roman CGI contains a contrast error budget for its black silicon apodizers (Balasubramanian et al. 2015). The diffuse, hemispherical scatter off the black silicon contributes $<10^{-11}$ contrast, so we can safely ignore it for our HWO telescope designs as well. As for specular reflectance, the Roman CGI project estimated the upper limit as 2×10^{-10} contrast for its apodizer designs but did not validate that model in the lab. For the HWO

coronagraph instrument that needs 1×10^{-10} total contrast, that upper limit is not negligible and requires further modeling and empirical validation. It is quite possible that the noisy estimates of the black silicon reflectance are too high or that the assumed model of a flat, specularly reflected wavefront from the black silicon is incorrect. If either of these are true, then the total dark zone contribution from the black silicon could be well below the needed 10^{-10} contrast level. This proposal aims to resolve this uncertainty with a dedicated experiment.

2.2.1 Black Silicon Fabrication

For high contrast coronagraphic masks, cryogenic reactive ion etching is preferred over the normal, room-temperature approach. Normal reactive ion etching does not yield anisotropic etch results (i.e. preferentially removing material in the ion acceleration direction, while minimally etching in lateral directions). This is because no sidewall passivation is taking place. Anisotropic etching can be accomplished by two different techniques: i) the Bosch process, or ii) cryo etching. In the Bosch process, an etch (using sulfur hexafluoride, SF6) and passivation (using perfluorocyclobutane, C4F8) are cyclically iterated. The SF6 both etches the silicon and preferentially removes any deposited passivation material in the ion acceleration direction; thus, the passivation preferentially protects the sidewalls as the silicon is etched, enabling the formation of tall, vertical structures. However, experience has shown that it is extremely difficult to achieve uniform black silicon over large areas with the Bosch process. In the cryogenic etch process the two gases utilized are SF6 and oxygen (O2). At cryogenic temperatures the etch by products create the sidewall passivation layer. This is a continuous process (i.e. no cyclic variation of the gases is required). And once the temperature is raised the passivation layer sublimates away, leaving a very clean silicon surface. For the black silicon etch, excess O2 is pumped in, creating an over-passivation condition. This material tends to pool, forming a randomized web micro mask pattern. The voids in the pool are where the etching occurs, thus creating the black silicon.

2.3 Minimum Feature Size in Apodizers

High contrast apodizer designs are thousands of design pixels in diameter, and to keep instrument mass tractably low it is desirable to have the apodizer diameter as small as possible. An accurate vector diffraction model is needed to predict how small apodizer pixels can be in a given distribution in order to still achieve $<=10^{-10}$ contrast.

It is well known that feature sizes on the order of a wavelength experience large amounts of vector diffraction, and that vector diffraction decreases rapidly as the feature size increases. But there are currently no guidelines on how large is large enough to safely ignore vector diffraction at the 10^{-10} contrast level.

For a binary apodizer design to provide higher contrast, a larger outer working angle (OWA), or both, it needs more samples across in order to control higher spatial frequencies. It should be noted that the apodizer feature size is not directly tied to the number of deformable mirror (DM)

actuators because the DMs and apodizer are typically separated by an optical relay that can magnify or demagnify the beam as needed. If the three LUVOIR-A APLC apodizers were sized to match the Roman CGI apodizers (17 mm diameter) and given enough resolution (5000-7000 pixels across) to still provide $<1\text{x}10^{-10}$ contrast in a scalar diffraction model, their pixels would have max widths of 2.4-3.4 microns. As shown in Figure 2-2, feature sizes this small for a 600 nm wavelength result in significant, lab-measured vector diffraction effects for a grayscale ramp converted to microdots (Zhang et al. 2018). The amplitude transmission versus fill factor for the error-diffused microdot pattern is expected to be 1:1 in a scalar model, but vector diffraction causes nonlinearity. Increasing the beam diameter to increase the apodizer pixel width adds significant mass and cost to a coronagraph instrument, so it is a limited strategy for reducing polarization aberrations.
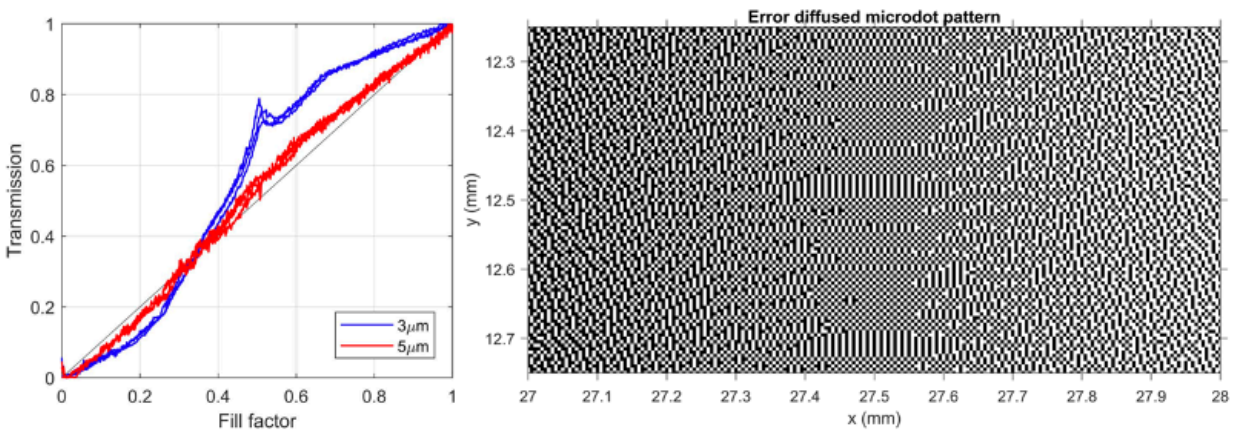
Figure 2-2. (Left) Lab-measured transmission versus fill factor for (right) an error-diffused, binary microdot pattern (Zhang et al. 2018). Scalar diffraction predicts a 1:1 ratio, but for the 600nm wavelength in this case, vector diffraction causes a large nonlinearity in the transmission for the 3-micron microdots and a smaller but still potentially problematic nonlinearity for 5-micron microdots.

For feature size, there are two different mask features to consider--the black silicon needle size and the width of the pixels in the apodizer mask design. Our established cryogenic black silicon process developed for coronagraph masks produces needles approximately 0.5-1.0 microns in diameter, so an apodizer pixel features presumably have to be a few times that width to produce the bulk material effect of being black. Regardless of the black silicon itself, even for a reflective apodizer, Figure 2-2 shows that a pixel width >8 times the wavelength is necessary for vector diffraction effects to be small. For the current proposed minimum HWO coronagraph wavelength of 350nm, that corresponds to >3 micron feature size. In other words, the minimum apodizer feature size we could expect to want would be several times larger than (and thus not limited by) the size of the black silicon micro-structures.

This project will develop and validate a vector diffraction model of the polarization aberrations generated by black silicon apodizers. This predictive model will be a valuable design tool when computing contrast error budgets for the HWO coronagraph instrument. To build a

representative 3-D vector diffraction model of a small region of the apodizer, we will take SEM measurements of (1) a region of black silicon needles and (2) of a transition region containing both an aluminized mirror region and a neighboring black silicon region. This will provide us with important parameters for the vector diffraction model such as the black silicon needle shape(s), height(s), lateral arrangement, and base depth(s) relative to the aluminized mirror.

3   Testbed Descriptions

3.1   Coronagraph Architecture

In the high contrast testbeds at JPL and the University of Arizona (UArizona), we will use apodizers in the SPLC architecture for this project. The main coronagraph types to consider are SPLCs, APLCs, and AVCs. Vector vortex masks are being developed in another SAT award and have not yet achieved $<1.6 \times 10^{-9}$ contrast (Ruane et al. 2022), so AVCs are not considered for this project.

There is a subtle difference between the APLC and SPLC, which is that the SPLCs have an outer field stop built into the FPMs to block most of the starlight. This greatly improves the robustness to alignment and magnification errors. For this reason and the SPLC heritage from Roman CGI, we will use the SPLC architecture for our tests. Importantly for risk reduction, the fabrication method for the metal-on-glass FPMs is the same for SPLCs, APLCs, and CLCs.

As part of this proposal, we aim to show that SPLC designs can simultaneously deliver high contrast, high throughput, and workable IWAs. This is possible with an off-axis aperture because the apodizer does not have to fight against large amounts of extra diffraction from struts or a secondary obscuration. Figure 3-1 shows one such high performance SPLC design for a clear, circular aperture as designed by the project's principal investigator (PI). It delivers 43% of the core throughput relative to the mask-less Airy pattern PSF and a mean contrast of 5×10^{-11} over the FPM opening from 3.5-29.0 λ/D in a 10% spectral bandwidth. This project includes design surveys to find other high-performance designs for monolithic and segmented input pupils.
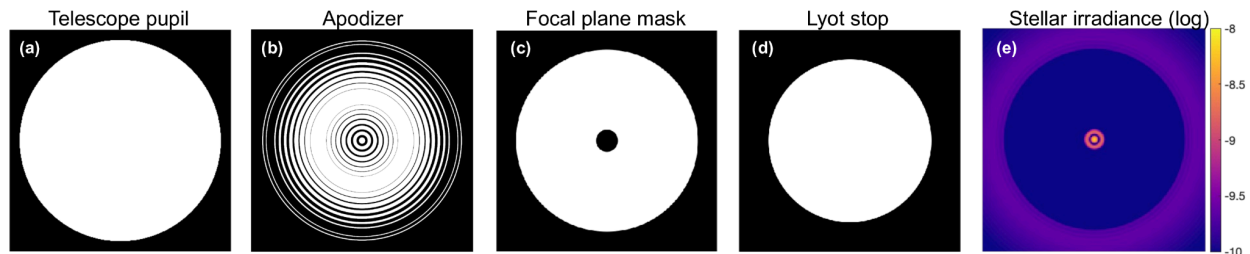
Figure 3-1. The key masks of a shaped pupil Lyot coronagraph (SPLC) design for an unobscured aperture. This design forms a 5×10^{-11} contrast dark zone from 3.5-29.0 λ/D over a 10% bandwidth and has a relative core throughput of 43% compared to an Airy pattern.

3.2   DST2 at JPL

As shown in Figure 3-2, JPL has two vacuum chambers containing its three high-contrast coronagraph benches–the Occulting Mask Coronagraph (OMC) testbed formerly used by Roman CGI, the Decadal Survey Testbed (DST), and the Decadal Survey Testbed 2 (DST2).
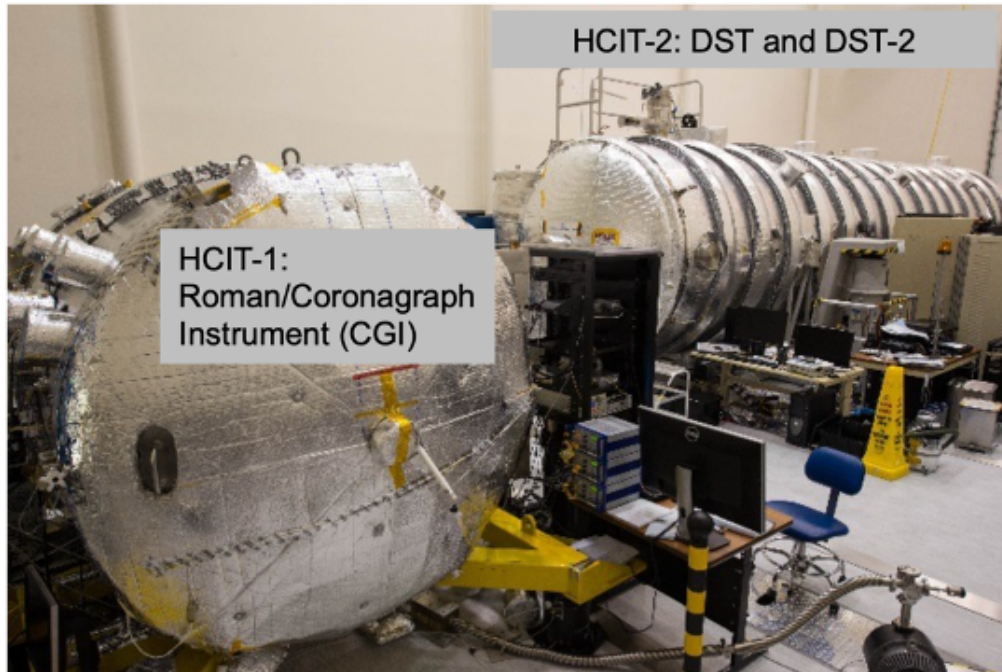
Figure 3-2. The vacuum chambers containing coronagraphic testbeds in JPL's HCIT.

The baseline plan is to perform all the milestone experiments on the vacuum-compatible DST2 bench in JPL's High Contrast Imaging Testbed (HCIT) facility. The optical layout of the DST2 is shown in Figure 3-3. The DST2 has the same optical layout as the original DST but with an additional set of relay optics upstream to provide a reflective pupil plane for apodizer masks (Meeker et al. 2021). There is only one DM, a 2k Boston Micromachines Corporation (BMC) device, in the DST2. The single DM limits the correctable dark zone to a 180-degree, half-plane region centered on the star when using conventional wavefront sensing and control (WFSC) techniques such as electric field conjugation (EFC) (Give'on et al. 2007). The DST2 has existing mounting locations for the FPM, Lyot stop, and field stop. The upstream reflective pupil plane currently has only a fold mirror, but it will be replaced as part of a facility upgrade with a mechanism to allow for multiple apodizers or a fold mirror to be used.
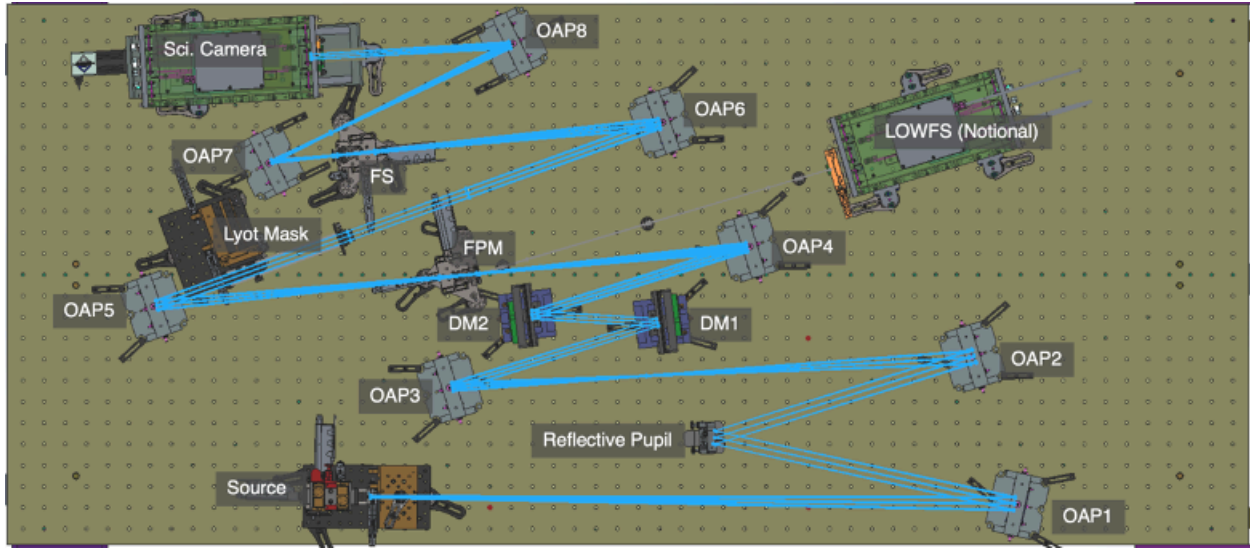
Figure 3-3. The labeled optical layout of the DST2 from Meeker et al. (2021). A reflective apodizer on lateral stages will be placed at the first pupil plane, labeled "Reflective Pupil." There is currently no DM2, just a fold mirror.

The combination of the DST2's current supercontinuum source, tunable filter, and single-mode fiber feed-through give it a usable input bandpass spanning ~530-670nm. Therefore, we plan to use a central wavelength of 600 nm to be in the middle of that range.

This project is not negatively impacted if there is just one DM available versus the two in Roman CGI and in the proposed HWO coronagraph instrument. Our coronagraphic hardware design and testing plan remains essentially the same because the DMs are meant only to perform wavefront correction with small stroke for the SPLC, which uses the masks to generate all the contrast. The WFSC software used in HCIT is set up to use either one or two DMs. Having two DMs just changes the ability to have a 360-degree versus a 180-degree azimuthal extent for the dark hole, so the only change needing prior planning would be to also include a fully circular field stop (versus just a half circle or half annulus) if a second DM were available.

There is no plan currently to add a second BMC DM to the DST2. The high-spatial-frequency BMC surface errors from a second, out-of-pupil DM would be highly chromatic and limit broadband contrast to around 10^{-9} to 10^{-8} (refer to Figure 10 from "High contrast imaging with MEMS deformable mirrors in the Decadal Survey Testbed", Riggs et al. SPIE 2021). In the medium future (e.g., 1-3 years), the DST2 front-end might be modified to use one or two 48x48 Xinetics DMs to avoid the BMC facesheet aberrations if they are deemed to be a major cause of the achievable contrast floor. The main concerns for the BMC DM facesheet is not achievable stroke but rather the periodic print-through (also called quilting) and sub-actuator ridges (called scalloping) resulting from flattening the DM surface.

3.3 Mask Reflectance Measurements at JPL

There is a much simpler optical bench at JPL for performing direct reflectance measurements of black silicon as shown in Figure 3-4 (Balasubramanian et al. 2015). It was used for the Roman CGI apodizer characterization with a HeNe laser (633 nm wavelength). If possible, we will swap in other lasers compatible with the existing neutral density (ND) filters and photodiode to obtain measurements at other wavelengths in the range relevant to HWO.
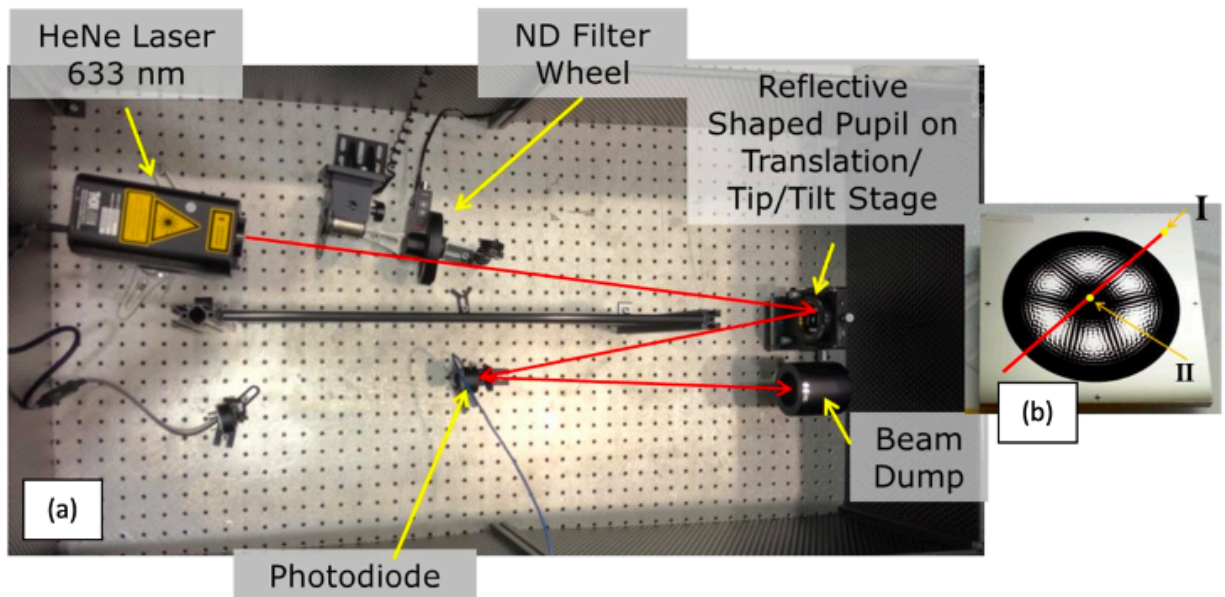
Figure 3-4. The JPL simple bench setup for measuring the reflectance of black silicon masks (Balasubramanian et al. 2015).

3.4 SCoOB at the University of Arizona

For faster mask testing and polarization model feedback, we plan to use the Space Coronagraph Optical Bench (SCoOB) at the University of Arizona (Ashcraft et al. 2022) as shown in Figure 3-5. It is a compact, vacuum-compatible coronagraphic testbed and can be used in vacuum as of 2023. SCoOB has reached 4×10^{-9} contrast in air and in vacuum in monochromatic light and 4×10^{-8} contrast in air in a 10% bandwidth (Van Gorkom et al. 2024 in prep). The facility goal (independent of this proposal) is to reach 1×10^{-9} contrast in vacuum. SCoOB has all the optical planes needed to include and test the masks of an SPLC. The SCoOB tests can be performed earlier and faster than at JPL, so they provide the opportunity for preliminary results up to one project phase earlier. It is important to note that the SCoOB tests are not strictly necessary and are meant to accelerate polarization model validation prior to the JPL tests.
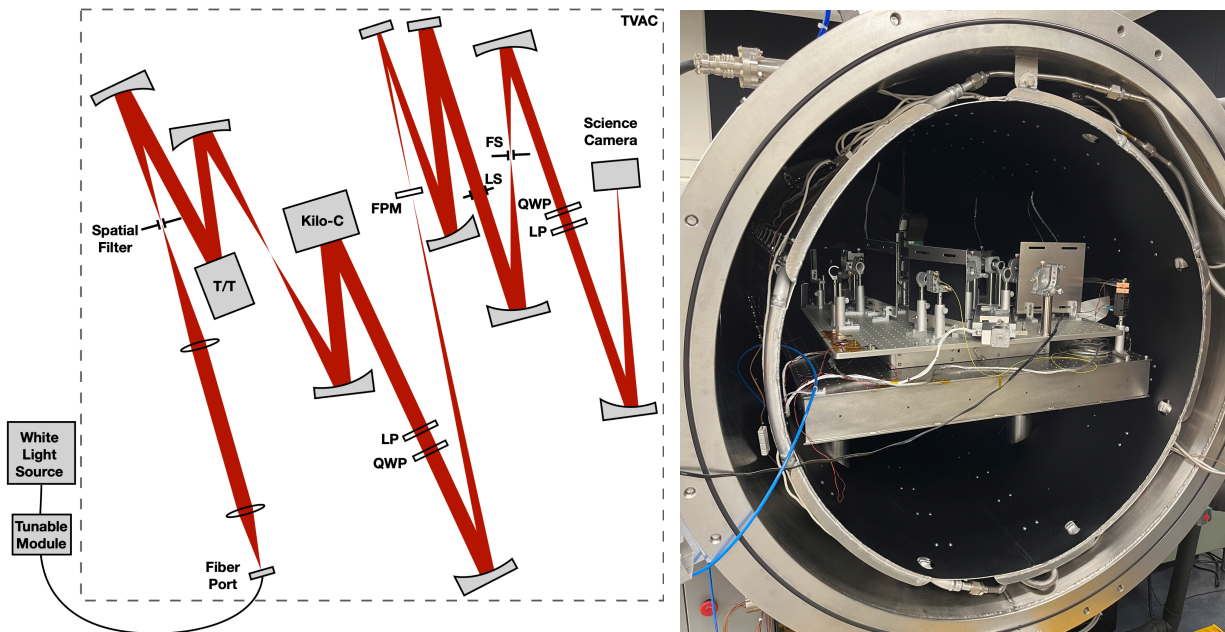
Figure 3-5. (Left) The optical layout of SCoOB at UArizona and (right) the testbed in the thermal vacuum chamber (Van Gorkom et al. 2024 in prep).

4 Technical Approach

At the heart of this proposal are several laboratory experiments to demonstrate apodizer performance and empirically validate models of vector diffraction for coronagraphic masks. In particular, this project will develop vector diffraction models for the black silicon apodizers, metal-on-glass FPMs, and through-hole Lyot stops used in the testbeds in order to determine the polarization aberrations expected from each and their potential interactions.

The technical plan has four phases. The first phase, tied to Milestone 1, differs in that it does not use WFSC and just involves characterizing the specular reflectance of black silicon.

The final three project phases each begin with mask design and modeling, and they culminate in high-contrast, vacuum-testbed experiments to meet one or two milestones per phase. The steps involved in each of these three high contrast testbed campaigns are listed below:

1. Mask design: Numerically optimize the apodizers, FPMs, and Lyot stops to be tested.
2. Predictive modeling check: Verify coronagraphic performance in closed-loop WFSC simulations of the testbeds. Re-optimize the masks to fix any issues found with them.
3. Mask fabrication: Order the black silicon apodizers from a new company run by former JPL MDL employees with the required expertise and/or directly from JPL's MDL. Order the FPMs, Lyot stops, and field stops from established outside vendors. Optically characterize the masks at JPL for surface figure error with a Zygo interferometer and for

lateral feature size errors and large particle contamination (>5-microns across) with a microscope.

4. <u>Testbed demonstration at the University of Arizona</u>: Perform model validation experiments to measure mask-induced polarization aberrations. This is to gather preliminary data to improve the vector diffraction models before the JPL tests.

5. <u>Testbed demonstration at JPL</u>: Perform coronagraphic WFSC in one of the JPL vacuum optical benches to reach as high a contrast as possible with the provided masks.

6. <u>Modeling to support and understand the testbed</u>: Per Exoplanet Exploration Program (ExEP) testbed policy, perform optical modeling during and after the high contrast tests to troubleshoot issues and to thoroughly understand observed performance.

7. <u>Milestone report writeup</u>: Immediately write up each milestone report in the form of an SPIE conference paper, to be presented and published at the next SPIE conference.

The vector diffraction model development will begin at the outset of the project and continue until the last milestone on model validation is completed. The differences among the four project phases are described in Section 4.1.

4.1 Project Schedule

The schedule in Figure 4-1 shows the work plan to achieve the technical milestones (shown as diamonds). The duration and level of effort for each task were determined based on the PI's prior experience performing design and modeling work for Roman CGI and performing modeling and testbed work for JPL's and Princeton University's high contrast coronagraphic testbeds.
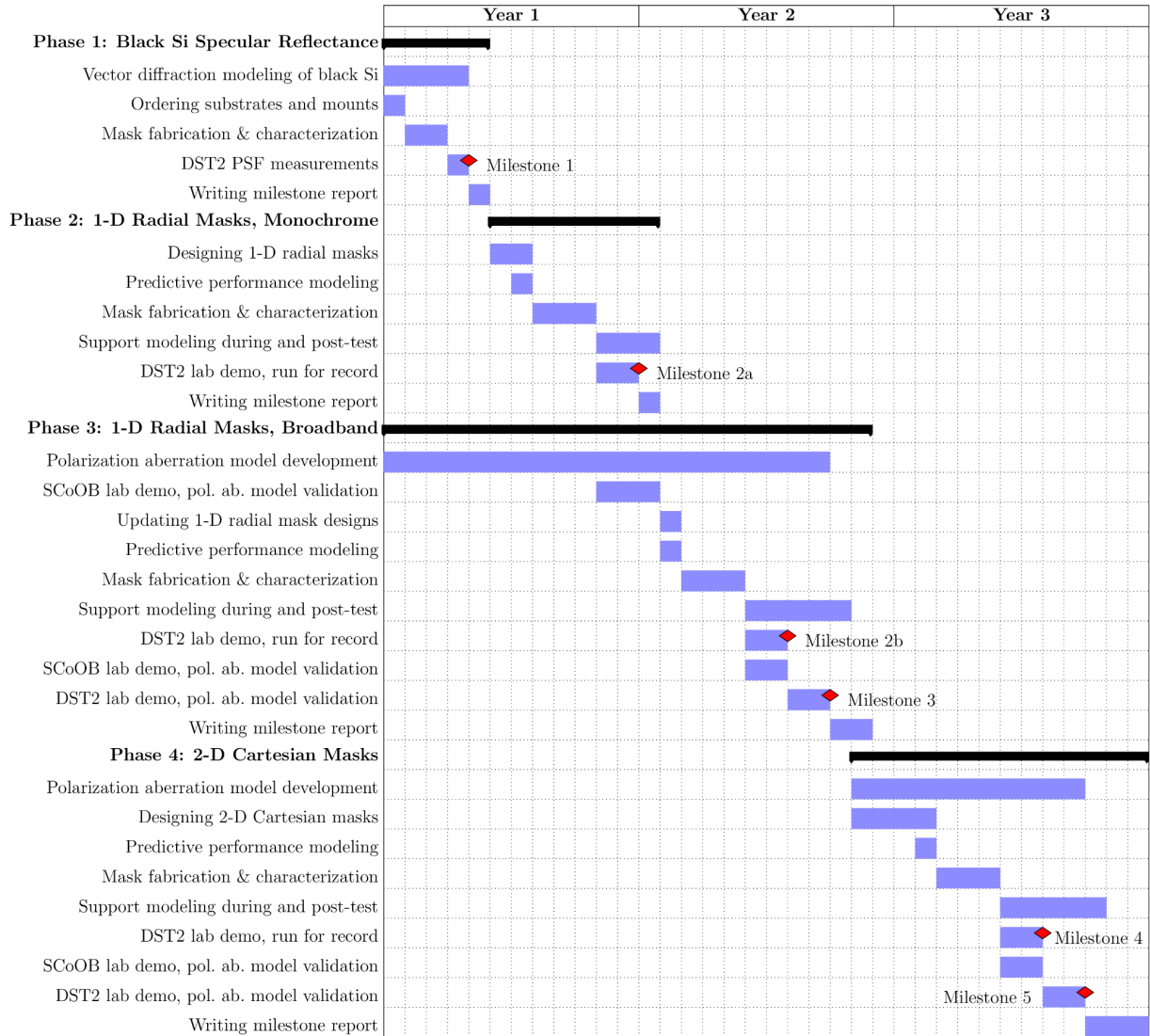
Figure 4-1. The schedule above shows the technical progression by task for the project.

4.1.1 Project Phase 1

The first phase of the project is tied to Objective 2 and Milestone 1. It is a standalone experiment to validate the model of specular reflection off black silicon. This first phase also provides preparatory time for the later project phases, such as polarization model development at UArizona and ordering long lead-time hardware for the testbeds.

4.1.2 Project Phases 2 and 3: 1-D Radial Apodizer Designs

Phases 2 and 3 are to demonstrate the best ever performance of apodizers for a clear, monolithic input pupil. The only milestone (2a) in Phase 2 is the easiest one to achieve, a monochromatic demonstration. Phase 2 is primarily intended as a trial run to flush out any

potential issues in the testbeds or mask designs that would require changes before the broadband demonstrations in Phase 3. Possible issues that may be found in Phase 2 include needing to reduce the apodizer diameter to block bad regions on the DM surface or finding a mismatch between the expected and true beam diameters and plate scales in the testbed.

All of the apodizer designs in Phases 2 and 3 will be circularly symmetric; that is, they will consist of concentric rings as shown in Figure 3-1. The 1-D design constraint drastically speeds up the mask optimization and allows millions of designs to be surveyed. In addition, the 1-D radial design simplifies the vector diffraction model development and validation for Milestone 3.

4.1.3 Project Phase 4: 2-D Cartesian Apodizer Designs

Phase 4 focuses on apodizers for a segmented input pupil in order to show compatibility with likely telescope architectures for HWO. Because the LUVOIR-B telescope is only slightly larger than the proposed HWO telescope, we plan to baseline the LUVOIR-B pupil for our Phase 4 apodizer designs. If there is an established telescope pupil for HWO by the time Phase 4 begins, we will switch to using that new aperture instead.

5 Milestones

Table 5-1 lists the five technical milestones and their main aspects. All relate to performance and/or modeling of black silicon apodizers. The requirements in common for Milestones 2-5 are that the focal plane dark zone must be somewhere in the wavelength range 400-1000 nm and have a spatial extent of a half-annulus from 4-10 λ/D centered on the star.

Table 5-1. Overview of the technical milestones in this proposal.

#	Month	BW	Testbed	Raw Contrast	Telescope Architecture	Milestone Name
1	4	20%	DST2	N/A	N/A; all black silicon	Model validation of black silicon reflectance at several wavelengths
2a	12	any	DST2	<5e-10	Clear monolithic	Monochromatic run for record with 1-D radial designs
2b	19	10%	DST2	<5e-10	Clear monolithic	Broadband run for the record with 1-D radial designs
3	21	10%	SCoOB & DST2	1e-9 to 1e-8	Clear monolithic	Model validation of polarization aberrations for 1-D optimized radial designs
4	31	10%	DST2	<5e-10	Segmented	Broadband run for the record with 2-D Cartesian designs
5	33	10%	SCoOB & DST2	1e-9 to 1e-8	Segmented	Model validation of polarization aberrations for 2-D Cartesian designs

5.1   Milestone Descriptions

Milestone 1 will satisfy Objective 2 by validating a model of how much light specularly reflected off a black silicon-only pupil mask lands in the focal plane within a radial separation of 10 λ/D from the stellar center, as compared to a flat, clear, fully metallized input pupil. The Roman CGI Milestone 1 report (Balasubramanian et al. 2015) only quantified the direct specular reflectance of black silicon. That will be measured first for our Milestone 1 as a reference point and to verify the initial quality of the black silicon samples. To determine the contrast error budget term in the focal plane dark zone, we will then look in the focal plane directly in one of the high contrast testbeds. The focal plane image of a purely black silicon pupil will be compared to that of a purely bare-aluminum pupil. We expect to see a faint, aberrated Airy pattern as the PSF for the black silicon pupil. For the modeling, we will perform finite-difference time-domain (FDTD) modeling of black silicon with the Meep package and build on prior published work performed for black silicon solar cells (Atteia et al. 2020).

To obtain several data points for Milestone 1 and more easily measure the wings of the black silicon pupil's PSF, we plan to fabricate and test black silicon samples with three different reflectance values. One sample will have the best possible $<10^{-7}$ reflectance typically used, and the other two will have intentionally worse reflectance values achieved by etching for shorter durations. The worse reflectance samples will be included to have more data points and to increase the chance of seeing any light in case the typical black silicon reflectance results in values too small to measure. We will perform these measurements in at least three narrow bands spanning the usable wavelength range of the testbed, currently ~530-670 nm.

Success for Milestone 1 will be defined as achieving model agreement within a factor of 2 in contrast for a 20% bandpass for the azimuthally averaged distribution of the black silicon-pupil PSFs out to 10 λ/D–for each of the black silicon samples with a different reflectance–divided by the peak measured value of the Al-pupil PSF. The black silicon reflectance model may be modified after data collection in order to match the observations more closely.

Milestones 2 and 4 are standard "run for the record" (i.e., do the best possible) lab demonstrations of $<=5\text{x}10^{-10}$ contrast to satisfy Objective 1. Section 7 provides more specifics of this procedure. Milestone 2 is split into two parts to enable a precursor, monochromatic design/fabricate/test cycle for troubleshooting the testbeds. Otherwise, all the other milestones require a $>=10\%$ spectral bandwidth.

Milestones 3 and 5 are model validation lab experiments to satisfy Objective 3. The laboratory part of Milestones 3 and 5 will be run like standard "run for the record" experiments for the chosen masks. We will dig closed-loop dark zones with SPLCs designed to reach $<=1\text{x}10^{-10}$ contrast in a scalar diffraction model but only 10^{-9} to 10^{-8} contrast in a vector diffraction model. The goal is to validate the expected mean raw contrast of the polarization aberrations to within a scale factor of 2. A scale factor accuracy requirement is chosen because it is usable at all contrast scales; an absolute tolerance of, for example, $+/-10^{-10}$ contrast uncertainty would be too tight for 10^{-8} level polarization aberrations but too loose for 10^{-10} level polarization aberrations. We will include three different apodizer designs per substrate to provide different targeted amounts of

polarization aberrations (negligible, medium, large) to obtain more data points for accurate model validation. These experiments will occur immediately after the Milestone 2b and 4 tests, respectively, so that any contrast degradation can be attributable only to the apodizers' polarization aberrations. The vector diffraction model will be used predictively to design the masks used in the experiments, but after data collection the model may be updated to improve agreement with the observations.

5.2   Contrast Error Budget

Although the desired contrast target for observing habitable exoplanets is 1×10^{-10}, the targeted contrast in the "run for the record" milestones in this proposal is $<5\times10^{-10}$. That is on par with the best-ever achieved contrast on the original DST bench in the HCIT plus uncertainties, and the DST2 was built to be as similar as possible to the DST (Meeker et al. 2021).

In Table 5-2, we copy the five-element contrast error budget presented by Seo et al. (2019) for their best-ever 4×10^{-10} broadband contrast result with a CLC on DST. We include another column and more rows to show how we plan to achieve $< 5\times10^{-10}$ broadband contrast on the DST2 with SPLCs in this proposal. The new DM electronics on DST2 and SPLC jitter robustness effectively zero out two large terms from the CLC contrast error budget, thereby creating room for new error budget terms specific to the black silicon apodizers. The values in the new error budget are initial best estimates and will be refined as part of this project. The separate terms are directly added (versus using a root sum of squares) to provide a worst-case estimate of the total contrast.

Table 5-2. Contrast error budgets for the CLC on DST and the proposed SPLCs on DST2.

Phenomenon	Measured DST Contrast with CLC (from Seo et al. 2019)	Expected DST2 Contrast with SPLC (this project)	Remarks
DM voltage resolution	9e-11	< 1e-12	DM electronics changed from 16-bit to 20-bit resolution
Chromatic control residual	9e-11	1.0e-10	DST2 has similar off-axis parabolas to DST, plus one extra optical relay.
Occulter ghost	1.0e-10	< 1e-11	SPLC FPM blocks the bright parts of the PSF, so the ghost will be greatly reduced.
Testbed line-of-sight jitter	4e-11	< 1e-12	SPLCs have much better jitter sensitivity than CLCs.
Diffuse background	5e-11	5e-11	Shared vacuum chamber for DST and DST2, so expect to see again.
Diffuse scatter off black silicon	N/A	< 1e-11	Based on Roman CGI Milestone 1 report.
Specular reflection off black silicon	N/A	<= 5e-11	Initial allowance. Higher throughput designs will have less black silicon and thus less reflected light off it.

Polarization aberrations	Unknown	<= 5e-11	Initial allowance. "Run for record" designs will have larger features to minimize this.
Apodizer feature size errors	N/A	<= 5e-11	Based on the <=0.1-micron feature size accuracy for Roman CGI apodizers.
Apodizer contamination	N/A	<= 5e-11	Dust particles at a pupil plane diffract energy to very large angles. The small number of large particles (>10um) on past apodizers have been dicing residuals, and wafers for this project are planned to be left undiced.
Other mask contamination	De minimis	De minimis	FPM can be cleaned if dust is near the occulter. Lyot stop and field stop are through-holes, which have virtually no surface area for contamination.
Coronagraph design contrast	< 1e-11	5e-11	-
Measurement uncertainty	Unknown	4e-11	10% total uncertainty assumed from photometry errors, detector calibration, and flux stability
Total Contrast	**3.8e-10**	**<= 4.6e-10**	

5.2.1 Mask Contamination

Particulate contamination is most concerning at the FPM, especially if it is within the dark hole region. However, the metal-on-glass masks are sturdy enough to withstand the traditional drop-and-drag cleaning method with a lens tissue and alcohol. The current occulters used in the DST and DST2 have had dust contamination and been successfully cleaned and re-tested at high contrast.

Contamination is negligible in the error budget for the Lyot stop and field stop masks, which are through holes, because there is virtually no surface area on which contamination can collect. If there is an unlikely dust particle on the hole edge, it has been modeled not to matter at the Lyot plane where a small particle at the edge of the several-mm diameter beam diffracts only a small amount of energy and at high angles. As for field stops, their small size means we make a grid of masks with alternates that can be used if one is found to be defective or dirty.

As for the apodizers, past HCIT and Roman CGI masks have been made to best effort, and then contamination has been measured and modeled. Otherwise, taking a statistical approach to contamination modeling is costly since it involves running many simulations of high resolution masks in closed-loop WFSC. But even in open loop, the modeled effects of the small number of observed contaminants has a very small effect (on the order of 1e-10 contrast or less), so it would be even less in closed loop–see for example Figures 17-19 in Balasubramanian et al. 2017. The largest apodizer contaminants have historically been bits of aluminum and silicon from dicing

the masks near the end of fabrication. For this project, we will leave the circular wafers undiced to improve the apodizer cleanliness.

The black silicon masks are not cleanable via the drop-and-drag method, which breaks the black silicon. Instead, they can only be lightly cleaned. Clean air can be puffed onto the masks but can only dislodge loosely attached dust. The masks can be resubmerged in the same chemical solutions used to clean them at the end of fabrication, but past experience has shown that it still does not remove the large particles deposited earlier in the fabrication process.

6 Computing and Software

6.1 Computers

For coronagraph design and scalar diffraction modeling, the JPL team members already have personal or shared ownership of several servers with sufficient cores and memory for these purposes. The UArizona team members also have their own computers and can utilize their institution's supercomputing cluster for larger calculations.

6.2 Software

All custom, unreleased software packages created or used by the team members in this proposal will be released as open-source on GitHub.

6.3 Coronagraph Design Software

The SPLCs will be optimized with the PI's existing coronagraph design software. The 1-D radial design survey code was used for past investigations such as those shown by Ruane et al. (2018). The 2-D Cartesian design survey code was used to optimize the baseline SPLCs for the Roman CGI (Riggs et al. 2017, 2021). Both the 1-D and 2-D optimization codes are written in the AMPL programming language (Fourer et al. 2006) and use the commercial solver Gurobi.

6.4 Software for WFSC and Scalar Diffraction

The HCIT at JPL uses several open-source packages for coronagraphic operations and modeling. Precision mask alignment will be done with the Coralign package (https://github.com/nasa-jpl/coralign) developed by the PI and others for Roman CGI.

WFSC in the HCIT is performed with the Fast Linearized Coronagraph Optimizer (FALCO) package developed by Riggs et al. (2018). The WFSC algorithms in FALCO that we will use are EFC, implicit EFC (Haffert et al. 2022, Haffert et al 2023, Milani et al 2024), and pairwise probing (Give'on et al. 2011).

When performing closed-loop scalar diffraction modeling of DST2, the PROPER (Krist 2007) software model of DST2 is used instead of the actual testbed to generate the coronagraphic images fed into FALCO.

The SCoOB testbed software is based on the open-source Compute and Control for Adaptive Optics (CACAO) architecture by Guyon et al. (2018) and is regularly released by the UArizona team (https://github.com/uasal/MagAOX-scoob). SCoOB high-order WFSC is generally performed using implicit EFC and the control code is shared publicly (https://github.com/uasal/lina).

6.5 Vector Diffraction Modeling Software

To model bulk polarization effects in the DST2 and SCoOB, Zemax and the open-source package HCIPy (Por et al. 2018) will be used. The DST2 and SCoOB were designed with small angles of incidence on all the optics to minimize polarization aberrations, but the exact expected contrast contributions will be computed for completeness.

The majority of the polarization aberration analysis will be for the edges and small features of the coronagraphic masks. We plan to use the commercial Lumerical package and/or the open-source Meep package (Oskooi et al. 2010), which has been used already to perform FDTD modeling for annular groove vortex masks (Konig et al. 2022) and sub-scale starshade masks accurately at the 1×10^{-10} contrast level (Harness et al. 2021). Our graduate student researcher has experience using Meep to model source pinholes.

6.6 Mask Hardware

All of the masks will be made by vendors that have been proven successful in prior JPL HCIT efforts. The super-polished, high-conductivity silicon wafer blanks needed for the black silicon apodizers will be ordered from QED optics, E.R. Precision Optical, and/or Coastline Optics. JPL's MDL or a new outside vendor founded by former MDL employees with the required expertise will manufacture the apodizers on those wafers. The anti-reflective (AR) coated fused silica substrates for the FPMs will be ordered from CVI or Edmund Optics, and then Opto-Line International will fabricate the FPMs. The Lyot stops and field stops will be through-hole masks etched out of standard silicon-on-insulator (SOI) wafers either by JPL's MDL or Opto-Line International.

The only new mounting hardware needed is for the apodizer. A custom mount will be fabricated in the JPL machine shop and be combined with two off-the-shelf linear stages with sufficient travel range to reach all the apodizers on each wafer. Custom adapter plates between the mount and each apodizer wafer will be machined or 3-D printed at the JPL machine shop.

6.7 Mask Design Strategy

The SPLCs for each testbed experiment will be designed to provide $< 10^{-10}$ contrast in a scalar diffraction model as well as a core throughput >=10%, an IWA <=4.0 λ/D, and a spectral bandwidth of >=10%. For the model validation milestones in which we want to induce large polarization aberrations, smaller features will be forced into the apodizer designs via such strategies as increasing the OWA or freezing some small features into the starting pupil for the apodizer optimizations. Conversely, to minimize polarization aberrations in the run-for-the-record milestones, larger apodizer features will be enforced.

6.8 Mitigating Risks and Uncertainties

In Table 6-1, we list the major risks and uncertainties associated with achieving our stated objectives and milestones. They relate mainly to the unknowns of the new testbeds and the new models we propose to develop.

Table 6-1. Technical risks and uncertainties and their proposed mitigations for this project.

Risk / Uncertainty	Proposed Mitigation
Polarization aberrations could limit achievable contrast in the "run for the record" experiments because the model validation occurs afterward.	Mask feature sizes will be made as large as possible in the "run for the record" apodizer designs with either explicit feature size constraints or implicit constraints such as a smaller OWA. In Phase 2 in SCoOB, we will perform the first broadband vector diffraction model validation to get feedback before making new masks for Phase 3. Time permitting, we will also perform a broadband test in DST2 in Phase 2.
A given apodizer design might not generate large enough polarization for the model validation experiments.	We will force the masks to have many small features. If there are not enough isolated features at the minimum feature size, the apodizer will be re-optimized with a smooth curvature constraint to ensure a smoothly varying apodization that will then be turned binary with error diffusion.
The black silicon morphology could be too complicated to model exactly in a vector diffraction model.	The diffuse reflectance and absorptivity of black silicon have already been modeled successfully with FDTD software by Atteia et al. (2020) and others. The next step is to improve the models to predict specular reflectance correctly as well.
FDTD modeling of the apodizer's polarization aberrations may be too computationally expensive over the full ~30mm mask diameter.	For designs with sufficient separation between small features, the vector diffraction calculations can be computed for isolated small regions, and then the E-fields could be combined with linear superposition. We will apply for supercomputing cluster time at UArizona, JPL, or NASA if deemed necessary. Otherwise, if small features are not isolated, we will determine how to approximate vector effects over a larger region.
UArizona's SCoOB testbed is new and might not reach its facility goal of 1e-9 contrast during the project timeline.	The SCoOB tests are a means of accelerating the vector diffraction model development and validation but are not strictly necessary. The SCoOB work effort would be redirected to more

	modeling and closer collaboration on the JPL testbed experiments.
DST2 with its BMC DM and has not yet demonstrated better than 2x10^{-9} contrast in a 10% bandwidth.	The current limitations of DST2 are planned for investigation in the summer of 2024 as part of a separate effort supported by HCIT infrastructure funding. The diameter of the apodizers could be reduced by up to 50% to underfill the BMC DM aperture. This would block most of the so-called surface scalloping along the outer controllable DM surface and still allow the specified OWA of 10 λ/D in the milestones. If the BMC DM is found to be a major limitation for achievable contrast, the DST2 front-end may be redesigned in coming years to use two 48x48 Xinetics DMs instead.

7   Data Measurement and Analysis

This section reiterates the standard measurement and analysis procedures used in past milestone white papers such as Wallace et al. 2023. Several minor changes have been made that were necessary for the specifics of this project. The only major change was modifying the milestone demonstration procedure in Section 7.4 not to have to start completely over (i.e., from scratch) for the second and third trials.

7.1   Statistical Confidence Definitions

The performance will be assessed in terms of statistical confidence of the measured normalized intensity to capture the impact of experimental noise and uncertainties. In the following paragraphs we define the terms involved in this process, spell out the measurement steps, and specify the data products.

7.1.1 Starting from Scratch

We define "starting from scratch" to mean that the DM is set to the predetermined voltage map providing approximately flat phase at the exit pupil with all masks out, and that all coronagraphic masks are realigned before wavefront control starts.

7.1.2 Star

We define the "star" to be a small pinhole illuminated with laser or narrowband light relayed via optical fiber from a source outside the vacuum chamber wall (e.g., a laser or a filtered supercontinuum white light source). The "small" pinhole is to be unresolved by the optical system; e.g., on DST2, the effective resolution is 18 μm at a wavelength of 550 nm making the pinhole unresolved with a diameter that is 20% of the angular resolution.

7.1.3 Algorithm

We define the "algorithm" to be the computer code that takes as input the measured speckle field image, and produces as output a voltage value to be applied to each actuator of the DM, with the goal of reducing the normalized intensity in a predefined dark zone.

7.1.4 Normalized Intensity (NI)

The "normalized intensity" (NI) is a dimensionless map representing, for each pixel of the detector, the ratio of its value to the value of the peak of the central PSF that would be measured in the same testbed conditions (light source, exposure time, Lyot stop, etc.) if the coronagraph focal plane mask were removed.

7.1.5 Raw Contrast

Milestone performance will be measured in terms of "raw contrast", which is the normalized intensity of the coronagraphic image with throughput loss accounted for at each field point. For a more exact definition, we use the following wording from John Krist in "Numerical Modeling of the Habex coronagraph," Proc. of SPIE Vol. 11117, 1111705 (2019):

> "The term *contrast* is used in this document to define the relative brightness of a pixel of residual starlight in the coronagraphic field or the relative brightness of a planet. When used to describe a planet's intensity, contrast is the observed flux of the planet divided by the observed flux of the unoccculted star. When used to describe field brightness at a given location (x,y), contrast is the intensity of the starlight in pixel (x,y) divided by the peak pixel value if the star were offset to (x,y). By this convention, a field pixel of contrast c would have the same brightness as the peak of a planet of contrast c. "

7.1.6 Mean NI

The "mean normalized intensity" is a dimensionless quantity that is the average value of the normalized intensity over the dark zone and spectral range adopted for the experiment.

7.1.7 Mean Raw Contrast

The "mean raw contrast" is a dimensionless quantity that is the average value of the raw contrast over the dark zone and spectral range adopted for the experiment.

7.1.8 Statistical Confidence

The interpretation of measured numerical intensity values shall take into consideration, in an appropriate way, the statistics of measurement (including detector read noise, photon counting noise, and dark noise) and the uncertainties in the measured intensity (including detector linearity and flux calibrations).

The milestone objective is to demonstrate with high confidence that the true contrast value in the dark zone, as estimated from our measurements, is equal to or better than the required threshold contrast value c_0. The estimated true contrast value shall be obtained from the average of the set of four or more contrast values measured in a continuous sequence (over an expected period of tens of minutes).

For example, our milestone with required mean contrast value of $c_0 < 5.0 \times 10^{-10}$ shall be demonstrated with a confidence coefficient of 0.90 or better. Estimation of this statistical confidence level requires an estimation of variances. Given that our speckle fields contain a mix of static and quasi-static speckles (the residual speckle field remaining after the completion of a wavefront sensing and control cycle, together with the effects of alignment drift following the control cycle), as well as other sources of measurement noise including photon detection statistics and detector noise, an analytical development of speckle statistics is impractical. Our approach is to compute the confidence coefficients on the assumption of Gaussian statistics, but also to make the full set of measurements available to enable computation of the confidence levels for other statistics.

At any time in the demonstration, the true contrast is subject to laboratory conditions, including the quality of the optical components, their alignment, any drift in their alignment over time, and the effectiveness of each wavefront sensing and control cycle. With each iteration, our nulling procedure attempts to improve the contrast value, thus compensating for any drift or changes in alignment that may have occurred since the previous iteration, and further variations may be expected due to experimental noise and any limitations in the algorithm. The data set built up from a sequence of such iterations will provide a distribution of contrast values, which will be regarded as Gaussian about a mean contrast for the data set. We therefore consider the mean contrast value as representative of the true contrast value for a data set, and the distribution of contrast determinations among the iterations within the data set as a combination of both random wavefront control errors and random measurement errors.

The mean contrast values and confidence limits are computed in the following manner. The average of one or more images taken at the completion of each iteration is used to compute the contrast value c_i. The mean contrast for a set of images taken in a given sequence is:

$$\hat{c} = \sum_{i=1}^{n} \frac{c_i}{n}$$

where n is the number of images in each set. The standard deviation σ_{each} in the contrast values c_i obtained for individual images within the set, which now includes both the measurement noise and the (assumed random) contrast variations due to changes in the DM settings for each speckle nulling iteration, is:

$$\sigma_{each} = \sqrt{\sum_{i=1}^{n} \frac{(c_i - \hat{c})^2}{n-1}}$$

Our estimate $\hat{c}$ is subject to uncertainty in the contrast measurements $\sigma_{mean} = \sigma_{each} / n$ and the independently-determined overall errors in photometry σ_{phot}. With the approximation that the contrast values have a Gaussian distribution about the mean contrast, the statistical confidence that the mean raw contrast is less than $c_o = 5$ x 10^{-10} is given by:

$$\sigma_{conf} = \frac{1}{\sqrt{2\pi}} \int_{-\infty}^{t} e^{-z^2/2} \, dz$$

where $t = (c_o - \hat{c})/\sigma$ *and* $\sigma =$ sqrt $[\sigma^2_{mean} + \sigma^2_{phot}]$. The values $\hat{c}$ and σ are the milestone metrics. The 90% confidence value is the value c_0 such that *conf(c_0)* = 0.9 according to the above equations.

7.2 Measurement of the Star Brightness

The brightness of the star is measured with the following steps.

7.2.1. Photometric Reference

To create the photometric reference, a representative sample of short-exposure (e.g., tens or hundreds of microseconds) images of the star is taken, with all coronagraphic elements other than the focal plane mask in place. The focal plane mask is laterally offset by approximately 7 λ/D, so as to transmit maximum stellar flux in the annular or semi-annular opening between the inner radius defined by the FPM and the outer radius defined by the field stop.

The images are averaged to produce a single star image. The "short-exposure peak value" of the star's intensity is estimated. Since the star image is well-sampled in the focal plane (the Airy disk is typically sampled by ~10 pixels within a radius equal to the full width half maximum), the star intensity can be estimated using either the value of the maximum-brightness pixel or an interpolated value representative of the apparent peak.

The sub-pixel lateral centering of the star on the detector is also computed from these images.

7.2.2 Peak Count Rate

The "peak count rate" (counts/sec) is computed for exposure times appropriate for the detector shutter, detector readout, and testbed laser-light flux level (typically in the tens of microseconds).

7.3 Measurement of the Coronagraph Contrast

Each measured image, in both NI and raw contrast, is obtained as follows:

7.3.1 FPM Alignment

The focal plane mask is centered on the star image. All other coronagraphic masks (apodizer, Lyot stop, and field stop) are already aligned.

7.3.2 Illuminated Frame Collection

An image (typical exposure times are ~ tens of seconds) is taken of the coronagraphic field (the suppressed star and surrounding speckle field). The dimensions of the target area is defined as follows, where λ is the central wavelength in the >= 10% spectral bandwidth and D is the diameter of the input pupil:

- The dark zone over which the raw contrast is scored will be a continuous half-annulus (i.e., 180-degree azimuthal coverage) centered on the star from radii of 4.0 λ/D to 10.0 λ/D.

7.3.3 Empirical Master Dark Frame

An empirical master dark frame having the same exposure time as the illuminated images is collected and computed with a temporary hardware change to prevent light from reaching the detector. Typically this involves moving the field stop to a fully obstructed position temporarily, collecting several dark frames at that exposure time, and then averaging them to create the master dark frame. This can be done ahead of time if the exposure times are fixed, or in real time.

7.3.4 Image Calibration

The image has the empirical master dark subtracted. Then, the image is normalized by the "peak count rate" to be in units of NI.

7.3.5 NI to Raw Contrast

The NI-to-raw-contrast conversion map is computed pixel-by-pixel using the optical model of the coronagraphic system with the measured centering and plate scales. (This can be done ahead of time.) This conversion map is multiplied to the 2-D image in units of NI to convert it to units of raw contrast.

The raw contrast image is averaged over the defined dark zone to produce the estimated mean raw contrast value. To be explicit, the contrast value is the sum of all contrast values, computed pixel-by-pixel in the dark field area, divided by the total number of pixels in the dark field area,

without any weighting being applied. All spectral subbands are normalized to give equal weighting to the mean value. A minimum of three subbands will be used per 10% total bandwidth, with the baseline being five subbands (e.g., 2% bandwidth per subband). The root mean square (RMS) contrast in a given area can also be calculated.

7.4 Milestone Demonstration Procedure

Per ExEP policy, all experimental trials to satisfy milestones will be repeated at least three times to prove stability and repeatability of the result. The procedure for performing three trials of each milestone demonstration is as follows. The first trial necessarily starts from scratch because there is no prior best setting available. However, for the following two trials, a more flight-like approach (i.e., the Roman CGI operations strategy) will be used to minimize wasted time. The system will be reset to scratch, the masks will be realigned, and then the DMs will be returned to the final voltage maps from the previous trial. The only strong justification for starting from scratch in later trials would be if the system underwent a major change such as an optical realignment or a change in masks in between trials.

7.4.1 Procedure for the Trials

7.4.1.1 System to Scratch

The optical system is set to scratch. An initial coronagraphic NI image is obtained as described in Section 7.3.

7.4.2.2 (Only for Trials 2+) Reapply DM Voltages from End of Last Trial

The final DM settings from the end of the last trial are reapplied to serve as the starting point. An initial coronagraphic NI image is obtained as described in Section 7.3.

7.4.1.3 Wavefront Sensing and Control

Wavefront sensing and control is performed to find settings of the DM actuators that give the required high-contrast in the target dark zone. This iterative procedure takes hours to days.

7.4.1.4 Final Image Collection

A number of contrast field images are taken after WFSC has ended. The result at this point is a set of NI images and raw contrast images. It is required that a sufficient number of images are taken to provide statistical confidence that the milestone contrast levels have been achieved.

8 Key Personnel

Dr. A J Eldorado Riggs of JPL is the PI of the proposed investigation and brings over ten years of experience developing instrumentation, software, and algorithms for the high contrast imaging of exoplanets. For Roman CGI, he was the Mask Design Lead and is the Alignment and Calibration Verification Lead. He wrote and maintains the open-source software package FALCO, which is used to run and simulate JPL's HCIT benches. For this project, Dr. Riggs will be the overall managerial and technical lead. He will also be responsible for the specific sub-tasks of SPLC mask design and closed-loop WFSC modeling.

Dr. Gregory Allan of JPL, Co-I, will be the primary DST2 operator for the project. He has played a major role in the commissioning and modeling of the DST2. For Prof. Dimitri Mawet's SAT award on WFSC and spectroscopy through a single mode fiber, he has been performing the testbed experiments and WFSC modeling. He has past experience with high-contrast imaging, adaptive optics, and BMC DMs.

Dr. Garreth Ruane of JPL, Co-I, will assist with and advise on testbed operation and WFSC modeling. He is currently the HCIT operations manager and main operator of the DST. He has over a decade of experience developing instrumentation for high contrast imaging and several years of experience running coronagraphic testbeds.

Dr. Daniel Wilson of JPL, Co-I, will advise and assist with mask fabrication and characterization. He has three decades of experience in designing, electron-beam fabricating, and characterizing diffractive optical elements, including fabricating multiple types of flight coronagraph masks for Roman CGI.

Dr. Jagmit Sandhu of JPL, Co-I, will perform the characterization of all the apodizers, including microscope imaging, Zygo measurements, and reflectance measurements. He performed this role for the flight apodizers for the Roman CGI. He has almost 20 years of experience developing advanced optical instrumentation at JPL.

Dr. Kunjithapatham (Bala) Balasubramanian of JPL, Co-I, will advise on the mask fabrication and help troubleshoot any potential issues that arise during apodizer fabrication. He was the Mask Fabrication Lead for the Roman CGI and has decades of experience with optical materials and microfabrication.

Dr. Karl Yee of an external LLC, Co-I, will be the apodizer fabrication lead. He has been fabricating black silicon apodizers since they were invented in 2013. He performs the black

silicon etching steps for the apodizers. He has over a decade of experience with black silicon and other microfabrication techniques.

Victor White of an external LLC, Co-I, will perform the microlithography for the apodizer masks. He has over 25 years of experience in microfabrication, including nearly 20 years of making precision coronagraphic masks.

Professor Ewan Douglas of UArizona, Co-I/Institutional PI, will manage the work effort at UArizona. He is the PI of the UArizona Space Astrophysics Lab and the SCoOB testbed.

Dr. Ramya Anche of UArizona, Co-I, will lead the vector diffraction modeling and develop the polarization aberration error budgets for both the DST2 and SCoOB testbeds. She has extensive experience modeling polarization for the Thirty Meter Telescope, the largest solar telescope in India, and the Roman CGI.

Emory Jenkins of UArizona, graduate student, will develop models of the polarization aberrations generated by the coronagraphic masks, in particular the apodizers, and run WFSC experiments on the SCoOB testbed. He is a graduate student and is currently using Meep to model the polarization aberrations generated by the pinholes commonly used as the pseudo-star in high contrast imaging testbeds.

9 References and Citations

J. N. Ashcraft, H. Choi, E. S. Douglas, et al., "The space coronagraph optical bench (SCoOB): 1. Design and assembly of a vacuum-compatible coronagraph testbed for spaceborne high-contrast imaging technology," in Space Telescopes and Instrumentation 2022: Optical, Infrared, and Millimeter Wave, L. E. Coyle, S. Matsuura, and M. D. Perrin, eds., 12180, p. 121805L, International Society for Optics and Photonics, SPIE, 2022.

F. Atteia, J. Le Rouzo, L. Denaix, D. Duch´e, G. Berginc, J. J. Simon, and L. Escoubas, "Morphologies and optical properties of black silicon by room temperature reactive ion etching," Materials Research Bulletin 131, p. 110973, 2020.

K. Balasubramanian, D. Wilson, V. White, R. Muller, M. Dickie, R. Ruiz, S. Shaklan, E. Cady, B. Kern, R. Belikov, O. Guyon, and N. Kasdin, "High contrast internal and external coronagraph masks produced by various techniques," in Proc. SPIE, 8864, p. 88641R, 2013.

K. Balasubramanian, E. Cady, et al., "WFIRST/AFTA coronagraph technology development milestone 1 final report: Reflective shaped pupil mask fabrication and characterization," milestone report, Jet Propulsion Laboratory, January 2015.

K. Balasubramanian, A.J. E. Riggs, E. Cady, et al., "Fabrication of coronagraph masks and laboratory scale star-shade masks: characteristics, defects, and performance," in Proc. of SPIE, 10400, 2017.

K. Balasubramanian, B.-J. Seo, K. Patterson, C. Mejia Prada, A. E. Riggs, H. Zhou, D. Moody, E. Cady, V. White, K. Yee, R. Muller, P. Echternach, F. Greer, and D. Wilson, "Critical characteristics of coronagraph masks influencing high contrast performance," in Proc. SPIE, 11117, 2019.

R. Belikov, A. Give'on, B. Kern, E. Cady, M. Carr, S. Shaklan, K. Balasubramanian, V. White, P. Echternach, M. Dickie, J. Trauger, A. Kuhnert, and N. J. Kasdin, "Demonstration of high contrast in 10% broadband light with the shaped pupil coronagraph," in Proc. SPIE, 6693, pp. pp. 66930Y–1 − 66930Y–11, Sept. 2007.

E. Cady et al., "Shaped pupil coronagraphy for WFIRST: high-contrast broadband testbed demonstration," in Proc. SPIE, 10400, p. 104000E, 2017.

C. Dorrer and J. D. Zuegel, "Design and analysis of binary beam shapers using error diffusion," J. Opt. Soc. Am. B 24, pp. 1268–1275, Jun 2007.

D. Fischer, B. Peterson, J. Bean, et al., "LUVOIR Final Report," tech. rep., NASA, 2019.

R. W. Floyd and L. Steinberg, "An adaptive algorithm for spatial grey scale," in Proc. Soc. Inf. Disp, 7, pp. 75–77, 1976.

R. Fourer, D. M. Gay, and B. W. Kernighan, AMPL: A Modeling Language for Mathematical Programming, Duxbury Press, 2nd ed., 2002.

B. S. Gaudi, S. Seager, B. Mennesson, et al., "Habitable Exoplanet Observatory Final Report," tech. rep., Jet Propulsion Laboratory, August 2019.

J. Gersh-Range, A.J. E. Riggs, and N. J. Kasdin, "Flight designs and pupil error mitigation for the bowtie shaped pupil coronagraph on the Nancy Grace Roman Space Telescope", Journal of Astronomical Telescopes, Instruments, and Systems 8(2), p. 025003, 2022.

A. Give'on, B. Kern, S. Shaklan, D. Moody, and L. Pueyo, "Broadband wavefront correction algorithm for high-contrast imaging systems," in Proc. SPIE, 6691, p. 66910A, 2007.

A. Give'on, B. Kern, and S. Shaklan, "Pair-wise, deformable mirror, image plane-based diversity electric field estimation for high contrast coronagraphy," in Proc. SPIE, 8151, p. 815110, 2011.

O. Guyon, A. Sevin, D. Gratadour, J. Bernard, H. Ltaief, D. Sukkari, S. Cetre, N. Skaf, J. Lozi, F. Martinache, C. Clergeon, B. Norris, A. Wong, and J. Males, "The compute and control for adaptive optics (CACAO) real-time control software package," in Adaptive Optics Systems VI, L. M. Close, L. Schreiber, and D. Schmidt, eds., 10703, p. 107031E, International Society for Optics and Photonics, SPIE, 2018.

S. Y. Haffert, J. R. Males, K. V. Gorkom, et al., "Advanced wavefront sensing and control demonstration with MagAO-X," in Adaptive Optics Systems VIII, L. Schreiber, D. Schmidt, and E. Vernet, eds., 12185, p. 1218581, International Society for Optics and Photonics, SPIE, 2022.

A. Harness, S. Shaklan, P. Willems, N. J. Kasdin, B. K. Balasubramanian, P. Dumont, V. White, K. Yee, R. Muller, and M. Galvin, "Optical verification experiments of sub-scale starshades," Journal of Astronomical Telescopes, Instruments, and Systems 7(2), p. 021207, 2021.

R. Juanola-Parramon, N. T. Zimmerman, L. Pueyo, M. Bolcar, G. Ruane, J. Krist, and T. Groff, "The LUVOIR Extreme Coronagraph for Living Planetary Systems (ECLIPS) II. performance evaluation, aberration sensitivity analysis and exoplanet detection simulations," in Proc. SPIE, 11117, 2019.

N. J. Kasdin, R. J. Vanderbei, D. N. Spergel, and M. G. Littman, "Extrasolar planet finding via optimal apodized-pupil and shaped-pupil coronagraphs," Astrophys. J 582(2), pp. 1147–1161, 2003.

L. Konig, O. Absil, M. Lobet, C. Delacroix, M. Karlsson, G. O. de Xivry, and J. Loicq, "Optimal design of the annular groove phase mask central region," Opt. Express 30, pp. 27048–27063, Jul 2022.

J. Krist, "PROPER: an optical propagation library for IDL," in Proc. SPIE, 6675, p. 66750P, 2007.

D. Marx, E. Cady, A. J. E. Riggs, C. Prada, B. Kern, B.-J. Seo, and
F. Shi, "Shaped pupil coronagraph: disk science mask experimental verification and testing," in Space Telescopes and Instrumentation 2018: Optical, Infrared, and Millimeter Wave, M. Lystrup, H. A. MacEwen, G. G. Fazio, N. Batalha, N. Siegler, and E. C. Tong, eds., 10698, pp. 446 – 454, International Society for Optics and Photonics, SPIE, 2018.

S. R. Meeker, M. Noyes, H. Tang, G. Ruane, C. M. Prada, E. Bendek, W. Baxter, B. Crill, A. J. E. Riggs, P. K. Poon, and N. Siegler, "The Twin decadal survey testbeds in the high contrast imaging testbed facility at NASA's jet propulsion laboratory," in Techniques and Instrumentation for Detection of Exoplanets X, S. B. Shaklan and G. J. Ruane, eds., 11823, pp. 322 – 334, International Society for Optics and Photonics, SPIE, 2021.

Pathways to Discovery in Astronomy and Astrophysics for the 2020s, Natl Academy Pr, 2021.

A. F. Oskooi, D. Roundy, M. Ibanescu, P. Bermel, J. D. Joannopoulos, and S. G. Johnson, "Meep: A flexible free-software package for electromagnetic simulations by the FDTD method," Comput. Phys. Commun. 181(3), pp. 687–702, 2010.

E. H. Por, S. Y. Haffert, V. M. Radhakrishnan, D. S. Doelman, M. van Kooten, and S. P. Bos, "High Contrast Imaging for Python (HCIPy): an open-source adaptive optics and coronagraph simulator," 2018.

E. H. Por, "Phase-apodized-pupil Lyot Coronagraphs for Arbitrary Telescope Pupils," Astrophys. J 888(2), pp. 127, 2020.

L. Pueyo, C. Stark, R. Juanola-Parramon, et al., "The LUVOIR Extreme Coronagraph for Living Planetary Systems (ECLIPS) I: searching and characterizing exoplanetary gems," 2019.

A. J. E. Riggs, N. T. Zimmerman, B. Nemati, and J. E. Krist, "Shaped pupil coronagraph design improvements for the WFIRST Coronagraph Instrument," in Proc. SPIE, 10400, p. 104000O, 2017.

A. J. E. Riggs, G. J. Ruane, E. Sidick, C. T. Coker, and B. D. Kern, "Fast Linearized Coronagraph Optimizer (FALCO) I. a software toolbox for rapid coronagraphic design and wavefront correction," in Proc. SPIE, 10698, p. 106982V, 2018.

A. J. E. Riggs, G. Ruane, C. A. M. Prada, D. S. Marx, and B.-J. Seo, "High contrast imaging with MEMS deformable mirrors in the Decadal Survey Testbed," in Techniques and Instrumentation for Detection of Exoplanets X, S. B. Shaklan and G. J. Ruane, eds., 11823(118230S), pp. 105 – 113, International Society for Optics and Photonics, SPIE, 2021.

A. J. E. Riggs, V. Bailey, D. C. Moody, et al., "Flight mask designs of the Roman Space Telescope coronagraph instrument," in Techniques and Instrumentation for Detection of Exoplanets X, S. B. Shaklan and G. J. Ruane, eds., 11823(118231Y), pp. 188 – 210, International Society for Optics and Photonics, SPIE, 2021.

G. Ruane, A. J. E. Riggs, C. T. Coker, et al., "Fast Linearized Coronagraph Optimizer (FALCO) IV. coronagraph design survey for obstructed and segmented apertures," in Proc. SPIE, 10698, 2018.

G. Ruane, A. J. E. Riggs, E. Serabyn, W. Baxter, C. M. Prada, D. Mawet, M. Noyes, P. K. Poon, and N. Tabiryan, "Broadband vector vortex coronagraph testing at NASA's high contrast imaging testbed facility," in Space Telescopes and Instrumentation 2022: Optical, Infrared, and Millimeter Wave, L. E. Coyle, S. Matsuura, and M. D. Perrin, eds., 12180, p. 1218024, International Society for Optics and Photonics, SPIE, 2022.

B.-J. Seo, K. Patterson, K. Balasubramanian, et al., "Testbed demonstration of high-contrast coronagraph imaging in search for Earth-like exoplanets," in Techniques and Instrumentation for Detection of Exoplanets IX, S. B. Shaklan, ed., 11117, pp. 599 – 609, International Society for Optics and Photonics, SPIE, 2019.

D. Sirbu, R. Belikov, E. Bendek, et al., "Multi-star wavefront control at the occulting mask coronagraph testbed: monochromatic laboratory demonstration for the Roman Coronagraph instrument," in Proc. SPIE, 12680, 2023.

D. Slepian, "Analytic solution of two apodization problems," Journal of the Optical Society of America 55(9), pp. 1110–1115, 1965.

J. T. Trauger and W. A. Traub, "A laboratory demonstration of the capability to image an earth-like extrasolar planet," Nature 446(7137), pp. 771–773, 2007.

K. Van Gorkom, E. S. Douglas, J. N. Ashcraft, S. Haffert, D. Kim, H. Choi, R. M. Anche, J. R. Males, K. Milani, K. Derby, L. Harrison, and O. Durney, "The space coronagraph optical bench (SCoOB): 2. Wavefront sensing and control in a vacuum-compatible coronagraph testbed for spaceborne high-contrast imaging technology," in Space Telescopes and Instrumentation 2022: Optical, Infrared, and Millimeter Wave, L. E. Coyle, S. Matsuura, and M. D. Perrin, eds., 12180, p. 121805M, International Society for Optics and Photonics, SPIE, 2022.

K. Van Gorkom et al., "The space coronagraph optical bench (SCoOB): 4. vacuum performance of a high contrast imaging testbed", Proc. of SPIE, June 2024 (in prep)

J. K. Wallace, G. J. Ruane, N. A. Raouff, et al., "Technology Milestone White Paper: Dual-Purpose Focal Plane Mask", https://exoplanets.nasa.gov/internal_resources/2885/, 2023.

S. D. Will, M. Perrin, E. H. Por, et al., "High-order coronagraphic wavefront control with algorithmic differentiation: first experimental demonstration," J. Astron. Telesc. Instrum. Syst 9(4), p. 045004, 2023.

M. Zhang, G. Ruane, J.-R. Delorme, D. Mawet, N. Jovanovic, J. Jewell, S. Shaklan, and J. K. Wallace, "Characterization of microdot apodizers for imaging exoplanets with next-generation space telescopes," in Space Telescopes and Instrumentation 2018: Optical, Infrared, and Millimeter Wave, M. Lystrup, H. A. MacEwen, G. G. Fazio, N. Batalha, N. Siegler, and E. C. Tong, eds., 10698, p. 106985X, International Society for Optics and Photonics, SPIE, 2018.

N. T. Zimmerman, A. J. E. Riggs, N. Jeremy Kasdin, A. Carlotti, and R. J. Vanderbei, "Shaped pupil Lyot coronagraphs: high-contrast solutions for restricted focal planes," J. Astron. Telesc. Instrum. Syst 2(1), p. 011012, 2016.

10   List of Acronyms and Abbreviations

All acronyms and abbreviations are defined in the main text, but they are defined again below for the reader's convenience.

- · AMPL: A Mathematical Programming Language (https://ampl.com/)
- · Astro2020: Decadal Survey on Astronomy and Astrophysics 2020
- · APD: (NASA's) Astrophysics Division

- APLC: apodized pupil Lyot coronagraph
- AR: anti-reflective
- AVC: apodized vortex coronagraph
- BMC: Boston Micromachines Corporation
- C4F8: perfluorocyclobutane
- CACAO: Compute and Control for Adaptive Optics
- CGI: Coronagraph Instrument (specifically the one for Roman)
- CLC: classical Lyot coronagraph
- CNT: carbon nanotube
- DM: deformable mirror
- DST: Decadal Survey Testbed
- DST2: Decadal Survey Testbed 2
- EFC: electric field conjugation
- ExEP: Exoplanet Exploration Program
- FALCO: Fast Linearized Coronagraph Optimizer
- FPM: focal plane mask
- FS: field stop
- FSM: fast steering mirror
- FDTD: Finite-difference time-domain (FDTD)
- HabEx: Habitable Exoplanet Observatory
- HCIT: High Contrast Imaging Testbed facility
- HWO: Habitable Worlds Observatory
- IROUV: infrared/optical/ultraviolet
- IWA: inner working angle
- JPL: Jet Propulsion Laboratory
- LLC: Limited Liability Corporation
- LOWFS: low-order wavefront sensor
- LUVOIR: Large Ultraviolet/Optical/Infrared Surveyor
- MDL: Microdevices Laboratory (at JPL)
- ND: neutral density
- NI: normalized intensity
- O2: oxygen
- OAP: off-axis parabola
- OMC: Occulting Mask Coronagraph testbed
- OWA: outer working angle
- PI: principal investigator
- PROPER: (*not short for anything*) the PROPER optical propagation library
- PSF: point spread function
- RMS: root mean square
- Roman: Nancy Grace Roman Space Telescope

- · SAT: Strategic Astrophysics Technology
- · SCoOB: Space Coronagraph Optical Bench
- · SF6: sulfur hexafluoride
- · SEM: scanning electron microscope
- · SPLC: shaped pupil Lyot coronagraph
- · TRL: technology readiness level
- · UArizona: University of Arizona
- · WFSC: wavefront sensing and control

11 Acknowledgements